Research on Chemical Intermediates
https://doi.org/10.1007/s11164-021-04548-x

A novel approach using plant embryos for green synthesis of silver nanoparticles as antibacterial and catalytic agent

Minh-Trong Tran[1,2] · Linh-Phuong Nguyen[3] · Dinh-Truong Nguyen[3] · T. Le Cam-Huong[2] · Chi-Hien Dang[1,2] · Tran Thi Kim Chi[4] · Thanh-Danh Nguyen[1,2]

Received: 16 April 2021 / Accepted: 15 July 2021

Abstract

The plant extract has been used extensively for biosynthesis of noble metallic nanoparticles due to cost efficiency and simple technology. However, influence of plant growth condition can induce changes in composition and content of bioactive compounds, leading to difficulty in reproducing the metallic nanoparticles. In this work, we first utilized the plant embryos (*Panax vietnamensis* embryos—PVE) cultured under laboratory condition as a biosource for the synthesis of silver nanoparticles (AgNPs). This method can reduce unwanted changes of bioactive composition in the plant. The formation of AgNPs was optimized to afford the best colloidal solution. The physicochemical properties were characterized using analysis techniques including X-ray diffraction (XRD), transmission electron microscopy (TEM), selected area electron diffraction (SAED), Fourier transform infrared spectroscopy (FTIR) and thermal properties. Size of crystalline AgNPs was determined in the range of 3–20 nm with a mean size of 10 nm. The applications were investigated for antibacterial and catalytic effect. The biosynthesized AgNPs exhibited high antibacterial

Minh-Trong Tran and Linh-Phuong Nguyen authors contributed equally to this study.

✉ Dinh-Truong Nguyen
truong.nguyen@ttu.edu.vn

✉ Chi-Hien Dang
dangchihien@gmail.com

✉ Thanh-Danh Nguyen
ntdanh@ict.vast.vn

[1] Graduate University of Science and Technology, Vietnam Academy of Science and Technology, 18 Hoang Quoc Viet, Cau Giay District, Hanoi, Vietnam

[2] Institute of Chemical Technology, Vietnam Academy of Science and Technology, 1A, TL29, Thanh Loc Ward, District 12 , 70000 Ho Chi Minh City, Vietnam

[3] School of Biotechnology, Tan Tao University, Long An Province, Vietnam

[4] Institute of Materials Science, Vietnam Academy of Science and Technology, 18 Hoang Quoc Viet, Cau Giay District, Hanoi, Vietnam

Published online: 22 July 2021

activity against *Bacillus subtilis*, *Staphylococcus aureus* and *Escherichia coli.* The excellent catalysis behavior of PVE-AgNPs has been investigated for the reduction of *o-, m-, p*-nitrophenols and toxic organic dyes including methyl orange, rhodamine 6G and rhodamine B. The effect of catalyst amount on the reaction performance was studied via kinetic investigation. This work unfolds a potential method for scalable reproduction of metallic nanoparticles.

Graphic abstract

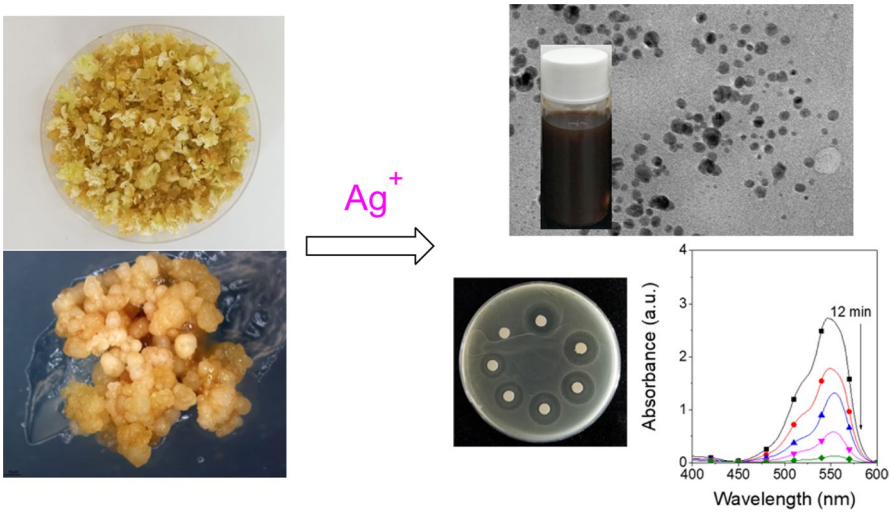

Keywords Silver nanoparticles · *Panax vietnamensis* embryos · Antibacterial agent · Catalyst · Nitrophenol · Pollutant degradation

Introduction

The outstanding properties of metallic nanoparticles have been used extensively in various advanced technology innovations ranging from agriculture to environmental fields [1–3]. Among them, silver nanoparticles (AgNPs) have been explored widely in optical sensing technology [4, 5], biotechnology [6, 7] and catalysis [8, 9]. Recently, AgNPs are frequently used as antibacterial and antifungal medicines against a broad range of microbial strains [10–12]. Also, it is well known as an effective catalyst for the degradation of numerous toxic contaminants via an electron transfer mechanism [13, 14].

AgNPs can be fabricated using different techniques such as γ-radiation [15, 16], laser ablation technology [17, 18] and chemical reduction [19]. Among them, the chemical reduction is the most useful and cost-effective method due to scalable fabrication and easy processing. Several common reductants such as hydrazine and sodium borohydride have been used frequently for the synthesis of AgNPs.

However, these chemical reductants have numerous disadvantages such as rapid reduction leading to great size and high toxicity which can limit applicable capacity in pharmaceutical and catalytic fields [20, 21]. Thus, it is highly desirable to fabricate AgNPs through eco-friendly and sustainable methods for these applications. Even though various green methods have been reported for the biosynthesis of AgNPs, the plant-mediated synthesis is well known as an effective technique due to cost efficiency, non-toxic reductants and biocompatible products [22–24]. However, composition and content of bioactive compounds presented in the plant extract are strongly dependent on numerous outside factors such as geography, soil condition and weather, which can lead to low producibility of metallic nanoparticles. Thus, the usage of the plant embryos grown under laboratory conditions for the fabrication of metallic nanoparticles is a new approach to address these disadvantages.

In this study, we first describe the fabrication of AgNPs from aqueous extract of *Panax vietnamensis* embryos which are cultured under controllable laboratorial condition. Its antibacterial activity is evaluated for inhibition of three bacterial strains. The catalytic activity is investigated for the reduction of nitrophenol derivatives and toxic dyes.

Experimental

Chemicals

All chemicals used were analytical grade without further purification. Chemicals including silver nitrate ($AgNO_3$), *o*-nitrophenol (*o*-NP), *m*-nitrophenol (*m*-NP), *p*-nitrophenol (*p*-NP), sodium borohydride ($NaBH_4$), methyl orange (MO), rhodamine 6G (Rh6G) and rhodamine B (RhB) were purchased from Acros Co. (Belgium).

In vitro culture of Panax vietnamensis embryos

Production of Callus samples *P. vietnamensis* roots were cut into thin cell layers with approximately 1 mm thick and cultured in MS medium supplemented with 2,4-dinitrophenylhydrazine (1.0 mg L^{-1}), sucrose (30.0 g L^{-1}) and agar (8.0 g L^{-1}) to develop the calli according to previous reports [25, 26]. The callus samples were cultured in fluorescent light of 45 µmol s^{-1} m^{-2}, temperature of 22 ± 1 °C and relative humidity of 50–60% in a photoperiod of 16 h. The pH medium was maintained in the range of 5.7–5.8 using NaOH solution (1 M) or HCl solution (1 M) for modification before autoclaving for 20 min at 121 °C. The white callus tissues were explanted to develop in 10 weeks for the formation of callus samples.

Production of embryo samples *P. vietnamensis* calli were cut into small pieces and cultured in SH medium supplemented with benzylaminopurine (1.0 mg L^{-1}), naphthaleneacetic acid (0.5 mg L^{-1}), hydrolysate casein (0.2 g L^{-1}), sucrose (30.0 g L^{-1}) and agar (8.0 g L^{-1}) [27]. The samples were cultured in the same conditions of the

callus procedure during 12 weeks to obtain the somatic embryos for the biosynthesis of silver nanoparticles.

Preparation of PVE extract

The PVE was dried at 60 °C for 24 h. The dried powder (10 g) was refluxed with 100 mL of distilled water for 1 h. The mixture was filtered, and the filtrate was stored in a refrigerator (4 °C) for further studies.

Optimization of AgNPs biosynthesis

The PVE extract was added to $AgNO_3$ solution by stirring in dark condition. Change in the color of solutions confirmed the AgNPs formation. The reaction parameters including concentration of Ag^+ ion (0–25 mM), reaction temperature (30–100 °C) and the reaction time (10–120 min) were optimized via measurement of UV–Vis spectra in the range of 250 to 600 nm. The reduction of silver ions induced an increase in absorbance at the peak of around 410–450 nm. The nanoparticles biosynthesized in the optimized condition were used for their physicochemical characterizations and applications. The solid AgNPs were obtained by centrifugation for 20 min at 4400 rpm and washed with water to remove silver ion and then acetone to remove the organic impurities. Finally, the nanoparticles were dried in an oven at 60 °C for 6 h.

Physicochemical characterization

For determination of the crystalline structure and composition of AgNPs, powder X-ray diffraction (XRD) analysis was carried out on a Shimadzu 6100 X-ray diffractometer (Japan). The FTIR spectra measured on a Bruker Tensor 27 FTIR spectrophotometer (Germany) in the range of 4000–500 cm^{-1} were applied to detect covalent bonds of possible functional groups presented in the PVE extract and powdered PVE-AgNPs. For evaluation of the size distribution and morphology of PVE-AgNPs, TEM (JEOL JEM-1400) and SEM (S-4800 HI-9057–0006) spectroscopy was used. The energy-dispersive X-ray spectroscopy (EDX) data were analyzed by an analyzer Horiba (EMAX ENERGY EX-400). The particle size and zeta potential of the AgNPs solutions were measured by using nanoPartica Horiba SZ-100 (Japan). Thermogravimetry analysis (TGA) and differential scanning calorimetry (DSC) were measured using a LabSys Evo 1600 thermal analyzer (SETARAM, France) in a temperature range from room temperature to 800 °C in the air atmosphere at a heating rate of 10 °C min^{-1}.

Antibacterial activity

Antibacterial test of the nanoparticles was carried out by using the disk diffusion method as previously reported [28]. *Bacillus subtilis* and *Staphylococcus aureus* as Gram-positive bacteria and *Escherichia coli* as Gram-negative bacterium were utilized to evaluate the antibacterial activity of the PVE-AgNPs

(1 µL) at different concentrations. Standard antibiotic ampicillin (0.01 mg/mL) and Luria–Bertani (LB) broth were used as positive and negative controls, respectively. Bacteria were taken out from storage and were cultured in LB broth at 37 °C for 6 h. After that, a sterile inoculating loop was used to streak bacteria on agar plates. The plates were incubated at 37 °C for 24 h. The colonies on the plate were picked up and transferred to liquid media and cultured at 37 °C for 6 h. The culture mixture was gently mixed to create a homogenous suspension. Hundred microliters of cell suspension was taken out and mixed with 100 µL of trypan blue (0.4%). Trypan blue cell suspension was transferred to the chambers of the hemocytometer by a micropipette. The cells were counted under a microscope at 100 × of magnification. The number of live cells should be 100 to 200 in the counting chamber (live cells appear colorless and dead cells stain blue). If the number of live cells were less than 100 or more than 200, concentrating or diluting the initial sample needed. Subsequently, the total number of living cells in the culture mixture was calculated based on the number of cells counted. Then, the original culture mixture was diluted to a solution that had 10^7 cells per mL. Hundred microliters of diluted culture mixture (equivalent 10^6 cells) were spread on the agar plates to evaluate the antibacterial activity of nanoparticles. The plates were incubated for 24 h at 37 °C. Antibacterial activity was recorded via diameters of inhibition zone around the paper disks in millimeter.

Catalytic activity

The catalytic activity of AgNPs was evaluated by reduction of nitrophenols including *o*-NP, *m*-NP and *p*-NP and degradation of toxic dyes including MO, Rh6G and RhB with an excess amount of $NaBH_4$ in aqueous medium. The reduction of nitrophenols was carried out by adding $NaBH_4$ solution (0.5 mL, 0.05 M) into corresponding nitrophenols (2.5 mL, 0.1 mM), and the degradation of toxic dyes was carried out by adding $NaBH_4$ solution (0.5 mL, 0.025 M) into the corresponding toxic dyes (2.5 mL, 0.05 mM). Then, solution of PVE-AgNPs catalyst (1, 2, 3, 4, 5 µL) was added into the reaction mixture. The reactions were performed in the quartz cuvette and monitored via UV–Vis spectrophotometers. A decrease in the absorption intensity of relative peaks of *o*-NP (414 nm), *m*-NP (389 nm), *p*-NP (400 nm), MO (464 nm), Rh6G (524 nm) and RhB (549 nm) confirmed the reactions occurring. Because this work used a very high concentration of the borohydride with respect to the pollutants concentration and very low amount of nanocatalyst, the rate equation of pseudo-first-order reaction, $\ln(A_t/A_0) = -kt$, should be considered for reduction of nitrophenols and degradation of organic dyes. In this equation, k is the rate constant, t is the reduction time, $[A_0]$ is the pollutant concentration at $t = 0$ and $[A_t]$ is the pollutant concentration at time t. A ratio of $[A_t]/[A_0]$ was calculated from the absorption intensity of the maximum peaks of the relative compounds. The value k was determined from slope value of the straight line generated by plots of $\ln(A_t/A_0)$ according to the reduction time.

Results and discussion

Biogenic synthesis

A schematic route for green synthesis of AgNPs is illustrated in Fig. 1. The dried powder of PVE, which was cultured via two steps and collected after 22 culturing weeks, was refluxed with distilled water. It is well known that the plant extract contains a variety of active compounds (e.g., flavonoids, protein, polysaccharide, etc.) that can be responsible for reduction of silver ions to AgNPs. The mechanism of metallic nanoparticles formation includes mainly three stages: reduction of metallic ions, clustering and further nanoparticle growth [29]. The features of each stage depend upon the nature and concentration of reducing agents. For instance, the hydroxyl groups present in flavonoids can be responsible for the formation of AgNPs. The tautomeric transformation in the flavonoid structure from enol form to keto form can create reactive hydrogen atoms that reduce silver ions to AgNPs [30]. Thus, the present work investigated the formation of AgNPs to determine suitable condition for the synthetic process. The concentration and morphology of PVE-AgNPs were evaluated using UV–Vis measurement. The nanoparticles synthesized in the optimized condition were used to investigate physicochemical characterizations and applied for antibacterial and catalytic effects.

It is well known that the formation of AgNPs can affect significantly their physicochemical characterization and biochemical properties. Thus, the reaction condition of the biosynthesis should be explored carefully to evaluate morphology and concentration of formed AgNPs based on changes in surface plasmon resonance (SPR) of the particles in UV–Vis spectra. In the present work, three parameters of the biosynthesis process including Ag^+ ion concentration, temperature and time were used to study the optimization.

The UV–Vis spectra obtained with a change in the factors are shown in Fig. 2. The influence of Ag^+ ion concentrations on the formation of PVE-AgNPs (Fig. 2A) can be observed at peaks of around 435 nm. The exploration was carried out in the concentration range of 0–25 mM. The result revealed that the SPR peaks did not appear clearly at the low concentration range of Ag^+ ion (< 20 mM). An increase in the absorption intensity with concentrated Ag^+ ion indicates PVE-AgNPs

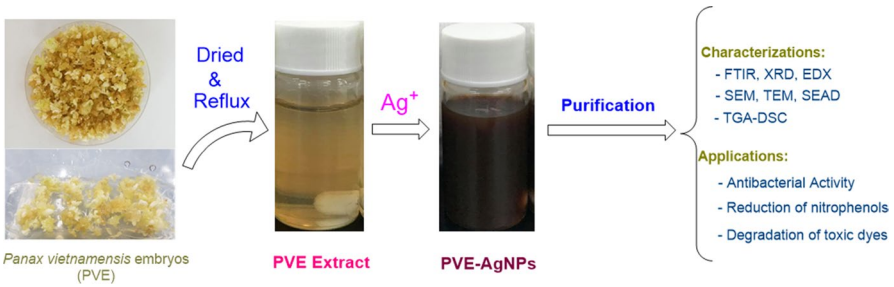

Fig. 1 Schematic illustration of biogenic synthesis of PVE-AgNPs

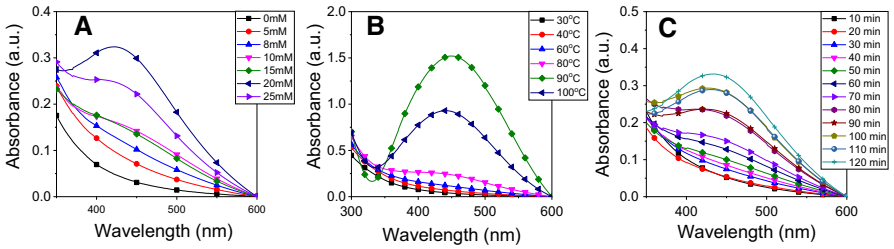

Fig. 2 UV–Vis spectra for effect of reaction condition on synthesis of PVE-AgNPs: **A** concentration of Ag^+ ion, **B** reaction temperature and **C** reaction time

concentration formed steadily increasing in the colloidal solution. Moreover, an increase in the Ag^+ ion concentration did not induce a change in absorption wavelength, which confirmed the stable morphology of the nanoparticles.

For the effect of reduction temperature, the synthesis of PVE-AgNPs was investigated in the range of 30 to 100 °C. The formation of AgNPs was only observed at high-temperature region (> 60 °C) where the SPR peak of AgNPs appeared clearly at around 440–450 nm. The results showed that the reducing activity of bioactive components in the PVE extract is similar to some other plant extracts as previously reported [28]. An increase in absorption intensity with increasing reaction temperature and achieving a maximum value at 90 °C indicated the strong dependence of AgNPs formation on the reduction temperature. The decrease in AgNPs concentration in colloidal solution at 100 °C relates to aggregation of AgNPs. The reduction in high-temperature requirement for the fabrication of PVE-AgNPs may be related to limited phytochemicals in the embryos as compared with fully grown plants [31].

The reduction time of Ag^+ ion was investigated in the range of 0–120 min with heating at 90 °C. The results are shown in Fig. 2C. The increase in absorption intensity with extending reaction time confirmed the higher concentration of the PVE-AgNPs in the colloidal solution. The formation of AgNPs is not observed for initial 60 min of stirring process. The SPR peak only appears clearly after stirring for 80 min. It is clear that the formation of AgNPs in the presence of PVE extract occurs slowly which can relate to the negative ions presented in the extract [32].

For further studies on their physicochemical characterizations and applications, the PVE-AgNPs were synthesized at the optimized conditions including silver ion concentration (20 mM), reaction temperature (90 °C) and reaction time (120 min).

Physicochemical characterizations of biosynthesized AgNPs

FTIR spectroscopy was used to identify the functional groups of bioactive compounds presented in the nanoparticles as the stabilization agents. The FTIR spectra of dried PVE extract and PVE-AgNPs are shown in Fig. 3. Both the spectra indicate absorption band similarly. Accordingly, the extract spectrum shows major bands at 3413, 2930, 1663, 1576, 1408 and 1072 cm^{-1}. The broad band centered at 3413 cm^{-1} is assigned to the stretching vibration of O–H and N–H groups which can relate to bioactive compounds such as polyphenols, flavonoids, polysaccharides,

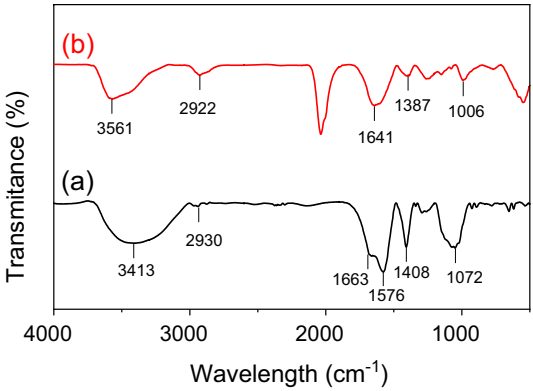

Fig. 3 FTIR spectra of PVE extract (**a**) and PVE-AgNPs (**b**)

proteins and alkaloids [33, 34]. The band at 2930 cm^{-1} is associated with C–H stretching vibration of polysaccharides and saponins. The strong band at 1630 corresponds to the stretch vibration of C = O bond relating to amides and carboxylic acid groups. The bands at 1408 cm^{-1} and 1072 cm^{-1} are associated with the stretching vibrations of C = C aromatic bond and C–O bond, respectively [35]. The spectrum of PVE-AgNPs shows the similar bands at 3561, 2922, 1641, 1387 and 1006 cm^{-1}. It reflects that the biomolecules act as the stabilization agents in the biosynthesis of nanoparticles.

Crystalline structure of PVE-AgNPs can be determined by using XRD analysis as shown in Fig. 4. The Bragg reflections of crystal AgNPs presented in the biosynthesized nanoparticles were found at 2θ values of 38.24°, 64.80° and 77.78° related to (111), (220) and (311) face-centered cubic (fcc) planes of AgNPs crystal, respectively (card no. 00–004-0783). On the other hand, the appearance of strong peaks at 27.62°, 32.32°, 46.10°, 54.91° and 57.30° corresponds to reflections from (111), (200), (220), (311) and (222) planes of crystal AgCl (card no. 00–001–1013) [36, 37]. Additionally, the lattice parameters of AgNPs and AgCl were found to be 4.0 and 5.5 Å, respectively (Table S2), which confirmed the presence of AgCl and AgNPs in the sample PVE-AgNPs [38, 39]. The AgCl crystal in the biosynthesized AgNPs can relate to the presence of chloride ion in the PVE extract which can be originated from culture medium and biosynthesis of PVE [32].

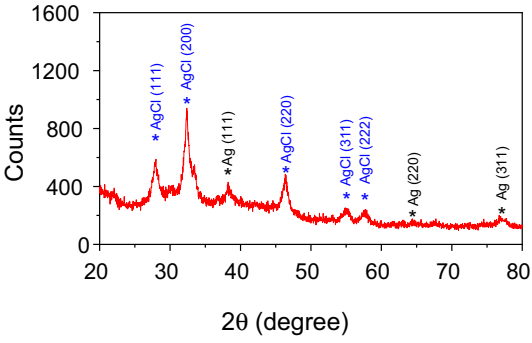

Fig. 4 XRD pattern of PVE-AgNPs

For study on morphology and elemental compositions of the PVE-AgNPs, SEM and EDX analysis of the powder sample was used. Particle size and crystalline nature were determined by TEM analysis and SAED pattern, respectively. The results are shown in Fig. 5. The SEM images confirm that PVE-AgNPs were

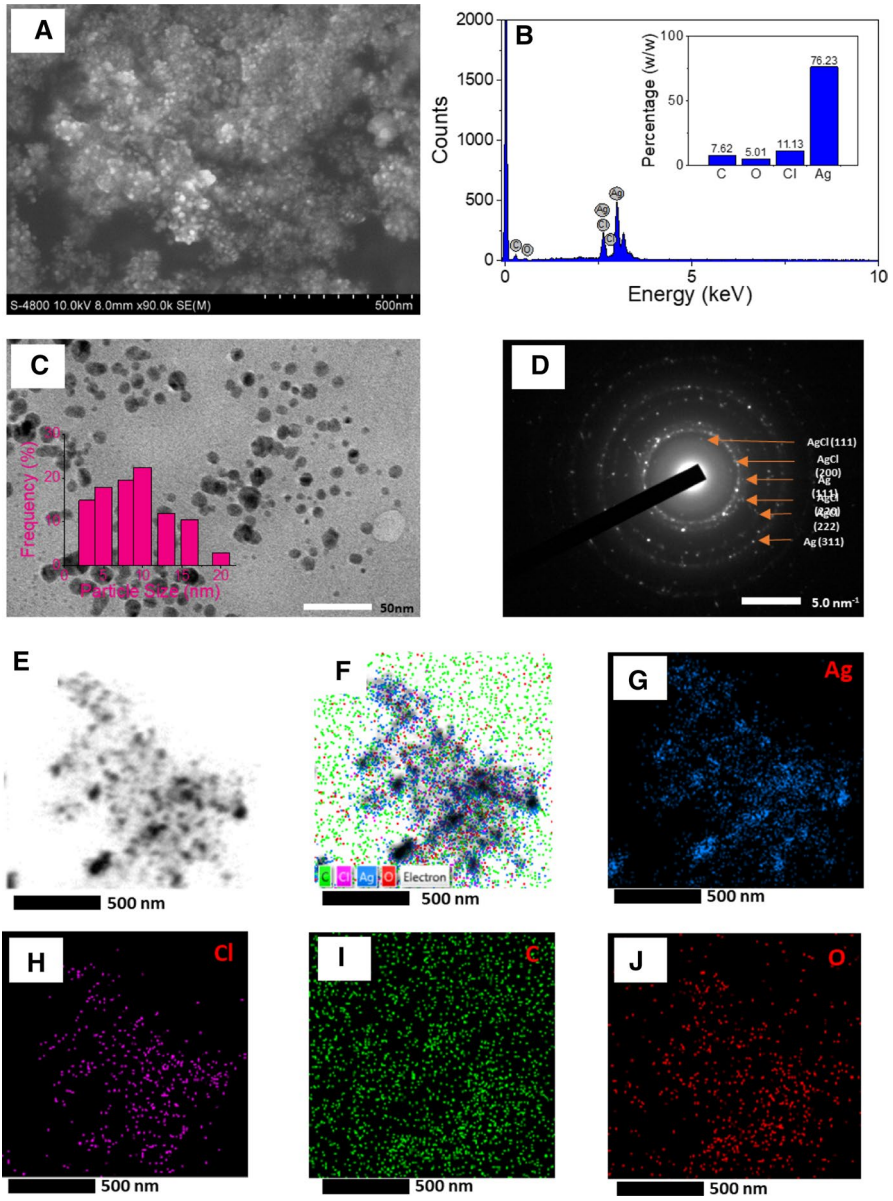

Fig. 5 **A** SEM image, **B** EDX pattern and elemental composition (inset), **C** TEM image and particle size distribution (inset), **D** selected area electron diffraction (SAED) pattern, **E** scanning transmission electron microscopy (STEM) and **F**–**J** elemental mapping of PVE-AgNPs

in a cluster manner formed from spherical particles with diameters below 25 nm (Fig. 5A). The EDX data reveal silver element presented in the solid sample that is confirmed by strongly elemental signals of 2.6 and 3.0 keV corresponding to binding energy of silver [40]. The bioactive organic composition in the sample is represented by carbon and oxygen elements. An intense peak at 2.7 keV is related to binding energy of chloride, which demonstrated the presence of crystalline AgCl in the sample [41]. Moreover, the EDX analysis shows the predominant composition of silver in the synthesized nanoparticles (76.23%, w/w) that promises to use effectively as bioactive and catalytic agents.

TEM analysis of PVE-AgNPs reveals an even geometry with the spherical particles (Fig. 5C) and narrow size distribution of nanoparticles is observed in the range of 3–20 nm with an average size of 10 nm. It indicates that the bioactive compounds in the PVG extract can stabilize effectively to form the nanoparticles with small size which can enhance activities of AgNPs. The SAED pattern shows bright rings corresponding to the crystalline nature of both AgNPs and AgCl. The circular rings are assigned to reflection planes of respective crystalline AgCl ((111), (200), (220) and (222)) and AgNPs ((111) and (311)), which is in agreement with the XRD data. The formation of composite Ag/AgCl has been observed in the biogenic AgNPs reported previously [42, 43]. The STEM and EDX mapping analysis (Fig. 5E–J) showed that elements, including silver, chloride, carbon and oxygen, indicated the presence of AgNPs, AgCl and organic components in the nanoparticles.

The thermal properties of PVE extract and the biosynthesized AgNPs were studied using TGA–DSC analysis. The result reveals the different thermal behaviors between the solid samples as shown in Fig. 6. The PVE extract showed the mass loss of 10% in temperature region below 100 °C that relates to the evaporation of water and volatile compounds and about 50% in temperature region of 200 °C, while the PVE-AgNPs sample is almost stable in this temperature region. It reflects that the biosynthesized nanoparticles do not possess volatile components. The extract is lost about 96% of weight at 800 °C, while the PVE-AgNPs showed about 40% of weight loss at this temperature region. The result of extract DSC showed endothermic peaks at low-temperature region, which confirmed evaporation process of the

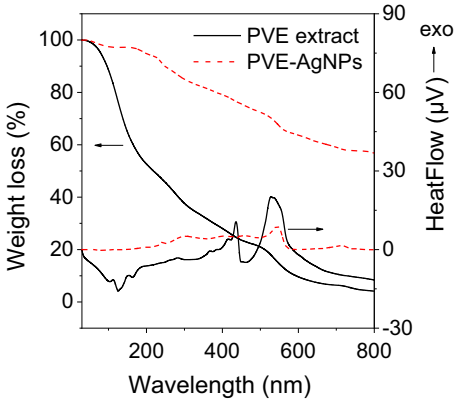

Fig. 6 TGA and DSC curves of PVE extract and PVE-AgNPs in air flow of 20 mL min^{-1} at a heating rate of 10 °C min^{-1}

volatile compositions. Both DSC curves of PVE extract and PVE-AgNPs showed the similar exothermic peaks at 280–300 °C, 445 °C and 540–550 °C, which are related to the oxidation of organic compositions. It confirms the organic molecules in the extract as stabilizing agents in the biosynthesized AgNPs.

Antibacterial assay

The antibacterial activity of PVE-AgNPs is evaluated against three microbial strains including *B. subtilis* and *S. aureus* (Gram-positive bacteria) and *E. coli* (Gram-negative bacterium) at various concentrations. The PVE extract also tested at the highest concentration exhibited no bioactivity against all the tested strains. The bioactivity of the biosynthesized PVE-AgNPs and plots of inhibition zone *versus* various concentrations are illustrated in Fig. 7. The result shows that PVE-AgNPs exhibit a good antibacterial activity against all tested bacteria and an increase in sample concentrations enhances their activity. The difference of bioactivity among the bacterial strains can be recognized at each test concentration. It can relate to antibacterial mechanism of AgNPs which strongly depend on the cell wall of each bacterial strain and membrane generation through hydrophobic and bioaccumulation mechanism [44]. The samples tested at concentration of 2.5 mM did not display any activity on all the strains, and the zones of bacterial inhibition grow when increasing

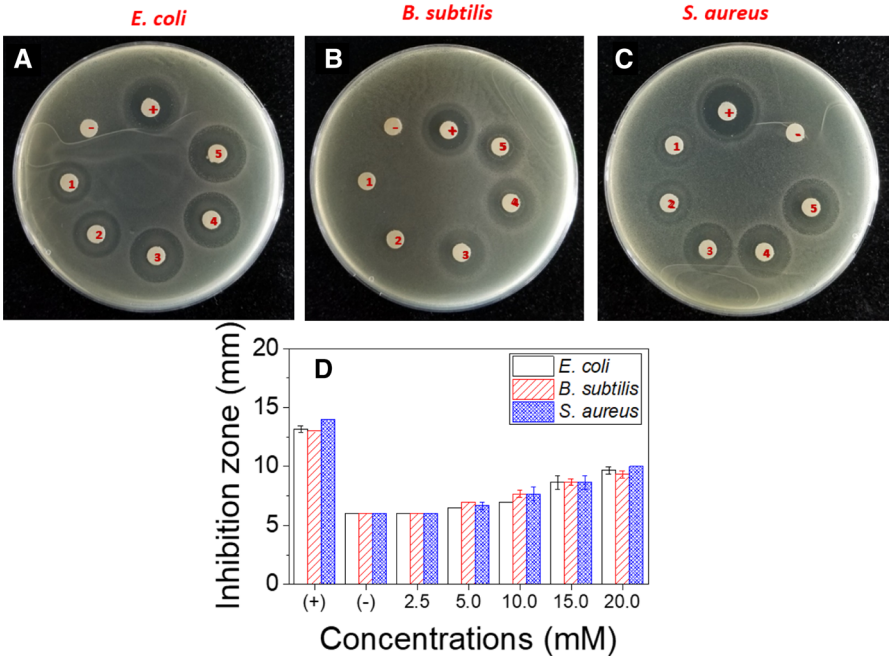

Fig. 7 Antibacterial activity of PVE-AgNPs tested at 1.0 µL of solutions with the different concentrations (2.5, 5.0, 10.0, 15.0 and 20.0 mM) against *E. coli* (**A**), *B. subtilis* (**B**), *S. aureus* (**C**) and plotting inhibition zone of various bacteria versus the different concentrations (**D**)

the concentration of PVE-AgNPs. Minimum inhibition concentration (MIC) values are found to be 5.0 mM for all the tested strains. PVE-mediated green synthesis of AgNPs showed similar activity to AgNPs biosynthesized from the plant extract [45–48]. Therefore, the PVE extract is suggested to use as a green source for the synthesis of metallic nanoparticles with potential applications in biotechnology.

Catalysis activity

The reduction of toxic organic pollutants including nitrophenols and dyes which pose serious threat to the living environment is widely considerable in environmental fields because they are not biodegraded in normally aqueous medium [13, 49]. Treatment of these toxic compounds can be performed by using various methods. Among them, the catalytic reduction using oxidizing and reducing agents such as H_2O_2 and $NaBH_4$ is reported frequently in the last decade. In the catalysis mechanism of the degradation using $NaBH_4$, the surface of AgNPs plays an important role as an absorbent of pollutant and BH_4^- ion where the electron transfer process occurs from BH_4^- (electron donor) to pollutant (electron acceptor) (Fig. 8). The catalytic performance of the nanoparticles is significantly dependent on several principle factors such as the surface of nanocatalyst, diffusion of the reactant, the binding ability between the catalyst and the reactant and desorption of the reaction products

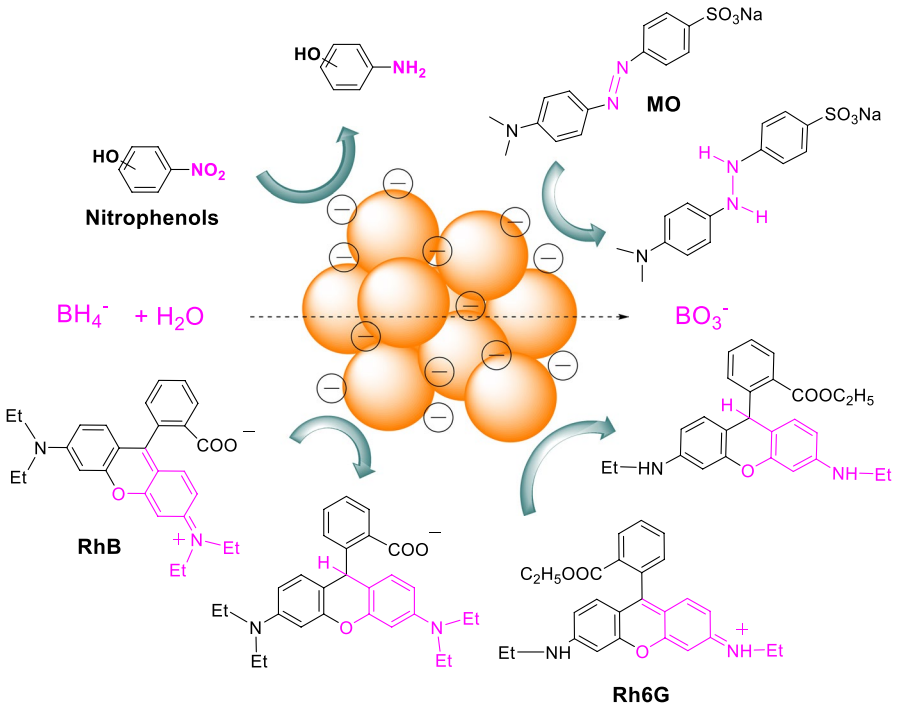

Fig. 8 Proposed mechanism of AgNPs catalysis in reduction of nitrophenols and organic dyes by $NaBH_4$

[32]. Otherwise, the catalytic behavior of the metallic nanoparticles is strongly dependent on the substrates and the amount of catalysts. Thus, the present study has investigated different substrates including *o*-, *m*-, *p*-nitrophenols, methyl orange (MO), rhodamine 6G (Rh6G) and rhodamine B (RhB) with the various doses of the nanocatalyst.

Reduction of nitrophenols

Reduction of nitrophenols into aminophenols (AP) not only pays considerable attentions in environmental field, but also possesses the potential applications in pharmaceutical technology. The AP derivatives are well known as key intermediates and precursors for numerous drugs such as pain treatment drugs (e.g., phenacetin, paracetamol, etc.) or sulfonamide drugs (sulfanilamide, protosil, etc.) [50]. The reduction kinetics of nitrophenols in the presence of PVE-AgNPs with a time-dependent manner of concentration were monitored in situ by measuring UV–Vis absorption from the cuvette. The reactions were confirmed by discoloration of the pollutant solution and decreasing absorbance values at relative peaks in the UV–Vis spectra.

Figure 9 illustrates the reduction of *o*-NP into *o*-AP in the presence of different doses of PVE-AgNPs solution (1–5 µL) which shows the degradation of absorption intention at peak 414 nm in UV–Vis spectra. An increasing reaction rate with the catalyst dose was confirmed via reduction of reaction time. The reduction of *o*-NP at 1 µL dose of the colloidal solution was completed in 27 min. However, reaction performance was increasing with 18 min in the presence of 3 µL PVE-AgNPs and even only taken 9 min at 5 µL PVE-AgNPs. For investigation of the kinetic, the plots of $\ln(A_0/A_t)$ values versus reaction time showed the good linear

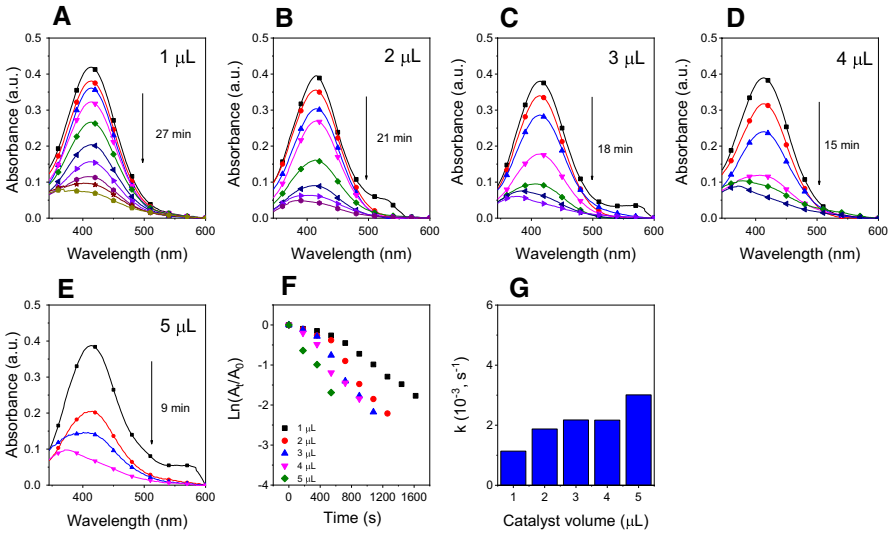

Fig. 9 UV–Vis spectra of *o*-nitrophenol reduction at different volumes of catalyst: 1–5 µL (**A**–**E**), plots of first-order kinetic (**F**) and rate constant values (**G**)

correlations for reduction of o-NP that coincided with the pseudo-first-order reaction (Fig. 9E). Furthermore, the rate constants calculated are quickly increased with high concentration of the nanocatalyst (Fig. 9F). The value calculated at 1 µL PVE-AgNPs is 1.14×10^{-3} s^{-1}, and this value is approximately double at 3 µL AgNPs (2.18×10^{-3} s^{-1}) and up to 3.01×10^{-3} s^{-1} at 5 µL PVE-AgNPs. It is clear that the total surface area of the nanocatalyst influences considerably the reduction behavior of *o*-NP.

For the reduction of *m*-NP, the absorption intensity at peak 398 nm is gradually reduced according to the reaction time after completing the addition of nanocatalyst. The slight influence of catalyst concentration on improvement in the reduction performance of *m*-NP is observed in Fig. 10. The result showed that the reduction yield was slowly increased from about 85% within 21 min in the presence of 1 µL PVE-AgNPs to 90% within 15 min at 3 µL PVE-AgNPs and achieved 90% within 12 min at 5 µL PVE-AgNPs. The study on the reaction kinetics showed the rate constants increasing with the nanocatalyst concentrations (Fig. 10F, G). The values were found to be 0.97×10^{-3} s^{-1}, 1.72×10^{-3} s^{-1} and 2.03×10^{-3} s^{-1}at 1 µL, 3 µL and 5 µL doses of PVE-AgNPs solution, respectively.

The similar trend is also found for the reduction of *p*-NP as shown in Fig. 11. Decreasing absorption intensity at peak 400 nm in UV–Vis spectra was observed according to the reaction time. The reduction of *p*-NP in the presence of PVE-AgNPs was completed more rapidly in comparison with the other nitrophenols. The reduction process was completed within 18 min at 1 µL and 2 µL doses, and the reaction time was achieved a maximum value of 12 min at 3 µL dose. Influence of catalyst amount on the reaction performance was not observed obviously when higher volume of the colloidal solution used. The similar result was also observed

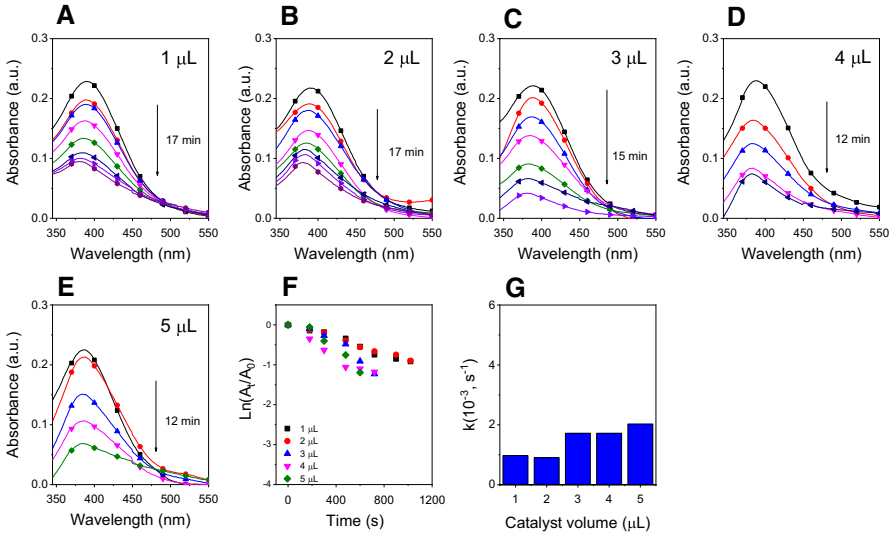

Fig. 10 UV–Vis spectra of *m*-nitrophenol reduction at different volumes of catalyst: 1–5 µL (**A**–**E**) plots of first-order kinetic (**F**) and rate constant values (**G**)

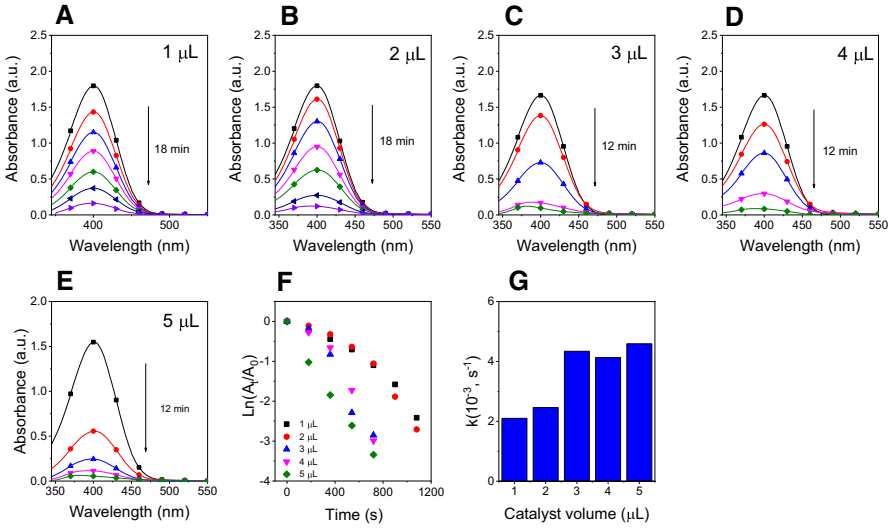

Fig. 11 UV–Vis spectra of *p*-nitrophenol reduction at different volumes of catalyst: 1–5 µL (**A**–**E**), plots of first-order kinetic (**F**) and rate constant values (**G**)

for the rate constants which were increased from 2.1×10^{-3} s^{-1} at 1 µL dose to 4.2×10^{-3} s^{-1} at 3 µL dose. In general, the best performance for reduction of *p*-NP was found at 3 µL dose of PVE-AgNPs used.

As given in Table 1, the reduction ability using PVE-AgNPs is increasing in the order of *m*-NP < *o*-NP < *p*-NP at each catalyst amount used. It is clear that the catalytic reduction of nitrophenols is dependent on the structure of substrates, which can be related to the diffusion ability of nitrophenol and desorption ability of aminophenol from the surface of catalyst. In comparison with AgNPs synthesized from plant extracts, plant embryo-mediated AgNPs in this work showed good efficiency for the reduction of nitrophenols [51–54].

Degradation of organic dyes

PVE-AgNPs catalyst was evaluated for degradation of three water-soluble dyes including MO, Rh6G and RhB which is used widely and become popular pollutants in industrial wastewater. The dyes with different structural characters possess various absorption peaks of 464 nm (MO), 524 nm (Rh6G) and 549 nm (RhB) in UV–Vis spectra even after the addition of $NaBH_4$ solution the peaks remained as same. The weak degradation of dyes without the catalyst can be observed after 30 min and reported elsewhere [55].

Methyl orange is an organic azo dye used commonly in various fields. MO is one important contaminant of wastewater that induces several environmental and health problems. Indeed, its degradation with low-cost and simple technique is paying attentions. The result revealed that the catalyst amount clearly influenced the reaction rate (Fig. 12). The completion of MO degradation was taken about

Table 1 Summary of rate constants for reduction of nitrophenols and dyes

Com	1 µL		2 µL		3 µL		4 µL		5 µL	
	k (10^{-3}, s^{-1})	R^2	k (10^{-3}, s^{-1})	R^2	k (10^{-3}, s^{-1})	R^2	k (10^{-3}, s^{-1})	R^2	k (10^{-3}, s^{-1})	R^2
2-NP	1.14	0.96	1.88	0.93	2.18	0.95	2.17	0.97	3.01	0.98
3-NP	0.97	0.97	0.90	0.99	1.72	0.90	1.72	0.94	2.03	0.90
4-NP	2.10	0.92	2.46	0.89	4.34	0.91	4.13	0.88	4.59	0.99
MO	2.09	0.94	3.25	0.89	2.82	0.92	3.35	0.97	4.15	0.96
Rh6G	0.38	0.99	1.01	0.99	2.06	0.86	3.21	0.90	3.54	0.91
RhB	2.16	0.91	2.73	0.86	4.08	0.87	4.02	0.91	12.60	0.94

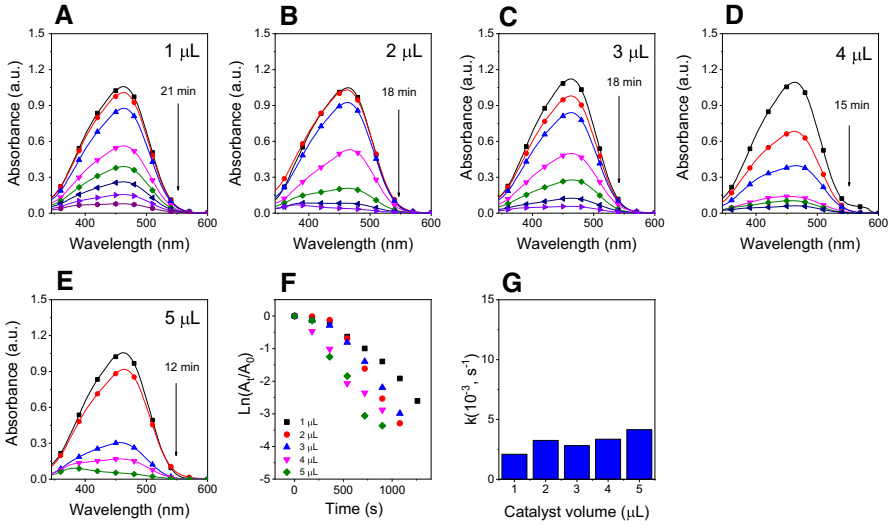

Fig. 12 UV–Vis spectra of methyl orange degradation at different volumes of catalyst: 1–5 µL (**A**–**E**), plots of first-order kinetic (**F**) and rate constant values (**G**)

21 min at 1 µL PVE-AgNPs, 18 min at 3 µL PVE-AgNPs and 12 min at 5 µL PVE-AgNPs. Good linear correlations between $\ln(A_0/A_t)$ values and the reaction times confirmed that the degradation of organic dye occurred via the pseudo-first-order reaction. Moreover, the increasing rate constants with catalyst amount were found to be 2.09×10^{-3} s^{-1} at 1 µL PVE-AgNPs, 2.82×10^{-3} s^{-1} at 3 µL PVE-AgNPs and 4.15×10^{-3} s^{-1} at 5 µL PVE-AgNPs.

Rhodamine 6G, a fluorescent dye, is used extensively in biotechnology fields. The detoxification of this contaminant is significantly considerable for wastewater treatment. The result indicated the reaction occurring much difficultly in comparison with other contaminants, which was confirmed by a slow decrease in the absorption intensity according to time at the same doses of the nanocatalyst (Fig. 13). The degradation was completed within more than 60 min at 1 µL PVE-AgNPs (70% yield in 60 min), 60 min at 2 µL PVE-AgNPs, 18 min at 3 µL PVE-AgNPs and 15 min at 5 µL PVE-AgNPs. The reaction kinetics showed that although the rate constants were increased with the catalyst amount, the rate constants were generally lower than the values of the other contaminants at the same dose. The values were found to be 0.38×10^{-3} s^{-1}, 2.06×10^{-3} s^{-1} and 3.54×10^{-3} s^{-1}at 1 µL, 3 µL and 5 µL doses of PVE-AgNPs solution, respectively.

Rhodamine B is widely employed in biotechnology and textile fields for various purposes and forms an important contaminant in wastewater. Due to great stability, its removal is highly desirable. The result revealed strong effect of the nanocatalyst amount on the degradation efficiency as shown in Fig. 14. The reaction was completed within 25 min at 1 µL PVE-AgNPs. When the nanoparticles amount was increased at 3 µL and 5 µL, the reaction time was significantly reduced within only 12 min and 6 min, respectively. The rate constant values were found to

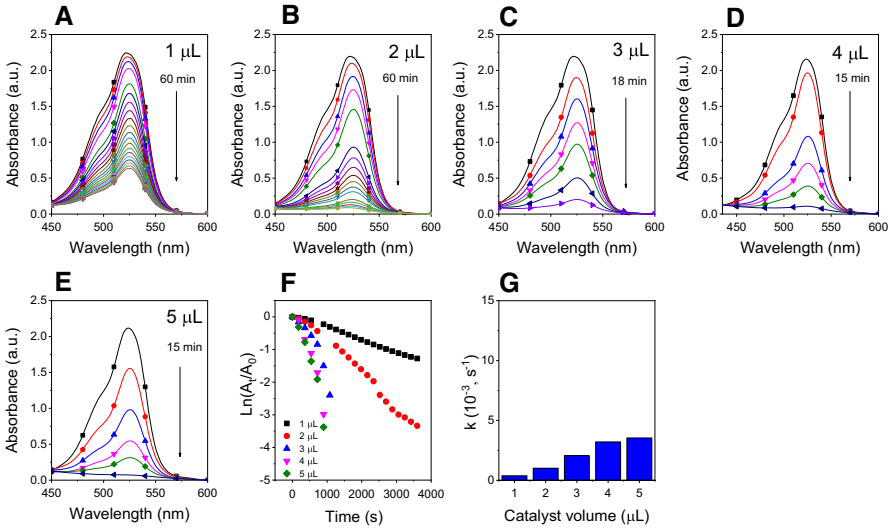

Fig. 13 UV–Vis spectra of rhodamine 6G degradation at different volumes of catalyst: 1–5 μL (**A**–**E**), plots of first-order kinetic (**F**) and rate constant values (**G**)

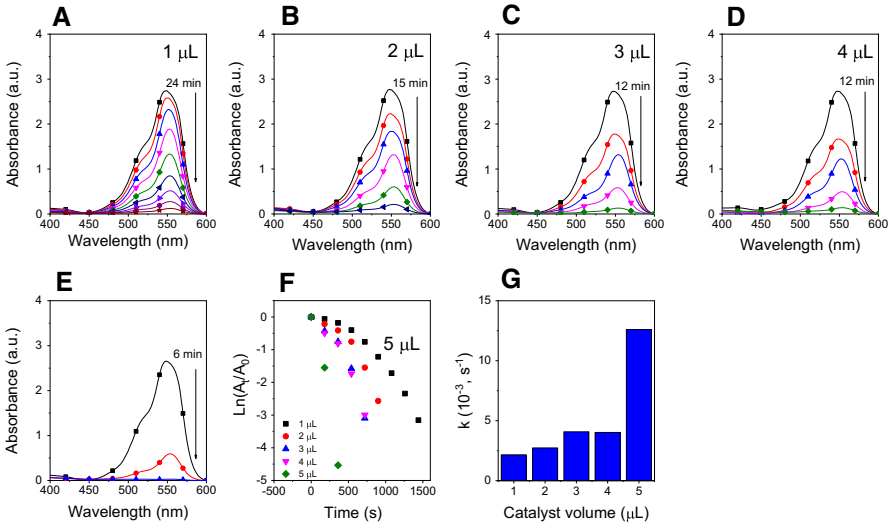

Fig. 14 UV–Vis spectra of rhodamine B degradation at different volumes of catalyst: 1–5 μL (**A**–**E**), plots of first-order kinetic (**F**) and rate constant values (**G**)

be 2.16×10^{-3} s^{-1} at 1 μL dose, 4.08×10^{-3} s^{-1} at 3 μL dose and 12.60×10^{-3} s^{-1} at 5 μL dose. In general, the degradation of RhB showed the highest catalytic efficiency among the organic dyes for all doses of PVE-AgNPs. Once again, the data confirmed the important effect of substrate structures on the catalytic degradation

using the metallic nanoparticles (Table 1). Moreover, AgNPs biosynthesized from plant embryos extract in this work indicated high catalysis performance of dye degradation in comparison with catalysts synthesized from plant extracts [55–58].

Conclusions

The present study demonstrated the plant embryos as a controllable biosource for eco-friendly synthesis of metallic nanoparticles. This approach can provide a new method for scalable production of metallic nanoparticles from the controllable laboratory condition. The silver nanoparticles were well characterized by the analysis technology of nanomaterials. The mean size of crystalline AgNPs was determined around 10 nm by TEM spectroscopy. The nanoparticles showed high activity against three tested bacterial strains. The MIC value was found to be 5.0 mM. The AgNPs catalyst showed good activity for reduction of nitrophenols and degradation of organic dyes. The reaction performance was improved significantly with an increase in the catalyst amount and influenced clearly by the substrate structures. The data showed that the reaction efficiency in the presence of nanocatalyst was increasing in the order of *m*-nitrophenol < *o*- nitrophenol < *p*-nitrophenol for reduction of nitrophenols and Rh6G < MO < RhB for degradation of organic dyes. Therefore, plant embryos-mediated synthesis can unfold a potential green method for the fabrication of nanometals as bioactive and catalytic agents.

Supplementary Information The online version contains supplementary material available at https://doi.org/10.1007/s11164-021-04548-x.

Acknowledgements This work was supported by Vietnam Academy of Science and Technology (No. NCVCC15.01/21-21).

Data availability statement The data used to support the findings of this study are included within the article.

Declarations

Conflicts of interest The authors declare that they have no conflicts of interest.

References

1. A. Sáenz-Trevizo, A. Hodge, Nanotechnology **31**, 292002 (2020)
2. A. Cartwright, K. Jackson, C. Morgan, A. Anderson, D.W. Britt, Agronomy **10**, 1018 (2020)
3. E. Hoseinzadeh, P. Makhdoumi, P. Taha, H. Hossini, J. Stelling, M. Amjad Kamal, Curr. Drug Metab. **18**, 120 (2017)
4. A. Jouyban, E. Rahimpour, Talanta **217**, 121071 (2020)
5. F. Mochi, L. Burratti, I. Fratoddi, I. Venditti, C. Battocchio, L. Carlini, G. Iucci, M. Casalboni, F. De Matteis, S. Casciardi, Nanomaterials **8**, 488 (2018)
6. M. Guilger-Casagrande, T. Germano-Costa, T. Pasquoto-Stigliani, L.F. Fraceto, R. de Lima, Sci. Rep. **9**, 1 (2019)
7. A.M. Othman, M.A. Elsayed, N.G. Al-Balakocy, M.M. Hassan, A.M. Elshafei, J. Genet. Eng. Biotechnol. **17**, 1–13 (2019)

8. Z.-J. Jiang, C.-Y. Liu, L.-W. Sun, J. Phys. Chem. B **109**, 1730 (2005)
9. K.D.O. Santos, W.C. Elias, A.M. Signori, F.C. Giacomelli, H. Yang, J.B. Domingos, J. Phys. Chem. **116**, 4594 (2012)
10. J. Talapko, T. Matijević, M. Juzbašić, A. Antolović-Požgain, I. Škrlec, Microorganisms **8**, 1400 (2020)
11. F. Behzad, S.M. Naghib, S.N. Tabatabaei, Y. Zare, K.Y. Rhee, J. Ind. Eng. Chem. **94**, 92–104 (2021)
12. N. Srikhao, P. Kasemsiri, N. Lorwanishpaisarn, M. Okhawilai, Res. Chem. Intermed. **47**, 1269 (2021)
13. S. Marimuthu, A.J. Antonisamy, S. Malayandi, K. Rajendran, P.-C. Tsai, A. Pugazhendhi, V.K. Ponnusamy, J. Photochem. Photobiol. B: Biol. **205**, 111823 (2020)
14. W.K.A.W.M. Khalir, K. Shameli, M. Miyake, N.A. Othman, Res. Chem. Intermed. **44**, 7013 (2018)
15. Y. Soliman, Radiat. Phys. Chem. **102**, 60 (2014)
16. L. He, L.F. Dumée, D. Liu, L. Velleman, F. She, C. Banos, J.B. Davies, L. Kong, RSC Adv. **5**, 10707 (2015)
17. M. Valverde-Alva, T. García-Fernández, M. Villagrán-Muniz, C. Sánchez-Aké, R. Castañeda-Guzmán, E. Esparza-Alegría, C. Sánchez-Valdés, J.S. Llamazares, C.M. Herrera, Appl. Surf. Sci. **355**, 341 (2015)
18. A.M. Brito-Silva, L.A. Gomez, C.B. De Araújo, A. Galembeck, J. Nanomat. **2020**, 142897 (2010)
19. B. Khodashenas, H.R. Ghorbani, Arab. J. Chem. **12**, 1823 (2019)
20. S. Iravani, H. Korbekandi, S.V. Mirmohammadi, B. Zolfaghari, Res. Pharm. Sci. **9**, 385 (2014)
21. J.A. Elegbede, A. Lateef, M.A. Azeez, T.B. Asafa, T.A. Yekeen, I.C. Oladipo, E.A. Adebayo, L.S. Beukes, E.B. Gueguim-Kana, IET Nanobiotechnol. **12**, 857 (2018)
22. M. Rafique, I. Sadaf, M.S. Rafique, M.B. Tahir, Artif. Cell. Nanomed. Biotechnol. **45**, 1272 (2017)
23. T.M.-T. Nguyen, T.T.-T. Huynh, C.-H. Dang, D.-T. Mai, T.T.-N. Nguyen, D.-T. Nguyen, V.-S. Dang, T.-D. Nguyen, T.-D. Nguyen, Res. Chem. Intermed. **46**, 1975 (2020)
24. N. Tarannum, Y.K. Gautam, RSC Adv. **9**, 34926 (2019)
25. T. Murashige, F. Skoog, Physiol. Plant. **15**, 473 (1962)
26. D. Nhut, B. Vinh, T. Hien, N. Huy, N. Nam, H. Chien, Afr. J. Biotech. **11**, 1084–1091 (2012)
27. R.U. Schenk, A. Hildebrandt, Can. J. Bot. **50**, 199 (1972)
28. T.-T. Vo, T.T.-N. Nguyen, T.T.-T. Huynh, T.T.-T. Vo, T.T.-N. Nguyen, D.-T. Nguyen, V.-S. Dang, C.-H. Dang, T.-D. Nguyen, J. Nanomat. **2019**, 8385935 (2019)
29. V. Borodina, Y.A. Mirgorod, Kinet. Catal. **55**, 683 (2014)
30. S. Jain, M.S. Mehata, Sci. Rep. **7**, 1 (2017)
31. M.A. Azeez, A. Lateef, T.B. Asafa, T.A. Yekeen, A. Akinboro, I.C. Oladipo, E.B. Gueguim-Kana, L.S. Beukes, J. Cluster Sci. **28**, 149 (2016)
32. V.-D. Doan, M.-T. Phung, T.L.-H. Nguyen, T.-C. Mai, T.-D. Nguyen, Arab. J. Chem. **13**, 7490 (2020)
33. B.K. Sharma, D.V. Shah, D.R. Roy, Mat. Res. Exp **5**, 095033 (2018)
34. N. Swilam, K.A. Nematallah, Sci. Rep. **10**, 1 (2020)
35. A.S.Y. Ting, J.E. Chin, Water Air, & Soil Pollut. **231**, 1 (2020)
36. M.S. Al Aboody, Artif. Cell. Nanomed. Biotechnol. **47**, 2107 (2019)
37. Z. Lou, B. Huang, P. Wang, Z. Wang, X. Qin, X. Zhang, H. Cheng, Z. Zheng, Y. Dai, Dalton Trans. **40**, 4104 (2011)
38. B. Mehta, M. Chhajlani, B. Shrivastava, Green synthesis of silver nanoparticles and their characterization by XRD. J. Phys.: Conf. Ser. **836**, 012050 (2017)
39. Ü. Akdere, Int. J. Mod. Phys. B **29**, 1550091 (2015)
40. B. Gowramma, U. Keerthi, M. Rafi, D.M. Rao, 3 Biotech. **5**, 195 (2015)
41. K. Okaiyeto, M.O. Ojemaye, H. Hoppe, L.V. Mabinya, A.I. Okoh, Molecules **24**, 4382 (2019)
42. H. Alishah, S. Pourseyedi, S.E. Mahani, S.Y. Ebrahimipour, RSC Adv. **6**, 73197 (2016)
43. S. Kota, P. Dumpala, R.K. Anantha, M.K. Verma, S. Kandepu, Sci. Rep. **7**, 1 (2017)
44. B. Khameneh, M. Iranshahy, V. Soheili, B.S.F. Bazzaz, Antimicrob. Resist. Infect. Control **8**, 1 (2019)
45. B. Ajitha, Y.A.K. Reddy, S. Shameer, K. Rajesh, Y. Suneetha, P.S. Reddy, J. Photochem. Photobiol., B **149**, 84 (2015)
46. A.R. Uddin, M.A.B. Siddique, F. Rahman, A.A. Ullah, R. Khan, J. Inorg. Organomet. Polym. Mater. **30**, 3305–3316 (2020)
47. M. Kgatshe, O.S. Aremu, L. Katata-Seru, R. Gopane, J. Nanomater. **2019**, 3501234 (2019)

48. M.N. Lakhan, R. Chen, A.H. Shar, K. Chand, A.H. Shah, M. Ahmed, I. Ali, R. Ahmed, J. Liu, K. Takahashi, J. Microbiol. Methods **173**, 105934 (2020)
49. A. Di Paola, V. Augugliaro, L. Palmisano, G. Pantaleo, E. Savinov, J. Photochem. Photobiol., A **155**, 207 (2003)
50. M.I. Din, R. Khalid, Z. Hussain, T. Hussain, A. Mujahid, J. Najeeb, F. Izhar, Crit. Rev. Anal. Chem. **50**, 322 (2020)
51. Z. Shah, S. Hassan, K. Shaheen, S.A. Khan, T. Gul, Y. Anwar, M.A. Al-Shaeri, M. Khan, R. Khan, M.A. Haleem, H. Suo, Mater. Sci. Eng. C, Mater. Biol. Appl. **111**, 110829 (2020)
52. K. Muthu, S. Rajeswari, B. Akilandaeaswari, S.M. Nagasundari, R. Rangasamy, Mater. Technol. https://doi.org/10.1080/10667857.2020.1786786 (2020)
53. B. Ajitha, Y.A.K. Reddy, Y. Lee, M.J. Kim, C.W. Ahn, Appl. Organomet. Chem. **33**, e4867 (2019)
54. L. Sherin, A. Sohail, U.S. Amjad, M. Mustafa, R. Jabeen, A. Ul-Hamid, Colloid Interface Sci. Commun. **37**, 100276 (2020)
55. T.-D. Nguyen, C.-H. Dang, D.-T. Mai, Carbohyd. Polym. **197**, 29 (2018)
56. A. Rajan, V. Vilas, D. Philip, J. Mol. Liq. **207**, 231 (2015)
57. F.K. Saidu, A. Mathew, A. Parveen, V. Valiyathra, G.V. Thomas, SN Appl. Sci. **1**, 1368 (2019)
58. Z. Shah, T. Gul, S. Ali Khan, K. Shaheen, Y. Anwar, H. Suo, M. Ismail, K.M. Alghamdi, S.M. Salman, Mater. Sci. Eng: B. **263**, 114770 (2021)